C-Coupon Studies of SiC/SiC Composites Part I: Acoustic Emission Monitoring

Gregory N. Morscher
Ohio Aerospace Institute
NASA Glenn Research Center, MS 106-5
Cleveland OH, 44135

Frances I. Hurwitz and Anthony M. Calomino
NASA Glenn Research Center
Cleveland OH, 44135

ABSTRACT

Modal acoustic emission (AE) was used to monitor the acoustic activity during room temperature and elevated temperature c-coupon tests for a variety of SiC/SiC systems including composites containing Sylramic®, ZMI™, or Hi-Nicalon™ fibers with melt-infiltrated or polymer-infiltrated SiC matrices. Modal AE proved excellent at monitoring matrix cracking in the curved portion of the C-coupon specimen with increasing load. This included the load at which the first AE event occurred and the location of AE events during the test that were, presumably, caused by the formation and growth of interlaminar cracks and, at higher loads, transverse cracks. Graphical techniques were employed to estimate the load for 1st AE. It was determined that for this test with these material systems, the first AE could be estimated within the load range bounded by the load at which initial deviation from linearity of the load-displacement curve occurs and the load where the 98% offset of the linear regression fit intercepted the load-displacement curve. The calculation of interlaminar tensile stress from the load for 1st AE was determined for all the systems. Ultimate ILT strength usually corresponded to ILT stress determined from the ultimate load to failure of the C-coupon test, which was considerably higher than the first cracking stress.

INTRODUCTION

The standard test technique used to measure interlaminar tensile (ILT) strength of composites is the tensile button test (ASTM 1468). This test technique, however, is currently limited to relatively low temperatures because epoxy is required as the adhesive for the specimen support rods. It would be desirable to measure high temperature ILT strength properties of ceramic matrix composites since these materials are envisioned for use at temperatures on the order of 1200°C. Therefore, a curved beam "C-coupon" test has been developed to assess the interlaminar strength properties of woven composites at elevated temperatures [1,2]. In these earlier studies, SiC/SiC composite C-coupon specimens were fabricated and a finite element analysis was performed, which demonstrated that the ILT strength of the C-coupon specimen could be determined

provided the ratio of ILT strength to axial tensile strength of the composite was less than the ratio of radial to hoop stresses for the C-coupon geometry.

Several issues still need to be resolved concerning the measurement of ILT properties by C-coupon tests versus ILT properties typically found from standard button tests. One of which is what load should be used to determine ILT strength when using the C-coupon test? Little if any non-linearity in the load displacement curve was observed for C-coupon tests even though significant amounts of both interlaminar and transverse matrix cracking were observed post-test. It is presumed in button tests that initial crack formation and growth leading to ultimate failure is a rapid process that occurs over a narrow load range. However, when and how much cracking occurred at what load is unknown for the C-coupon. Did most of the cracks in the C-coupon occur only close to failure (peak load), over a large load range, or after the load dropped when the arms (see Figure 1) of the C-coupon were rapidly pulled apart? If cracking occurs during the C-coupon test over a wide load range how should the load data be interpreted with respect to ILT strength determination? In order to answer these questions, the damage progression in the C-coupon needs to be understood. For this reason, acoustic emission (AE) was used in this study to determine when and where matrix or interphase cracking occurred during C-coupon testing on a number of different woven SiC fiber reinforced, SiC matrix composite systems.

The utility of AE to determine the onset of matrix cracking in ceramic composite tensile tests is well documented [3,4]. More recently, modal AE, i.e. the digitization and analysis of AE waveforms recorded with wide-band frequency transducers, enables accurate source location in a specimen and better source identification because the modes of the acoustic waveform, i.e. extensional and flexural, can be identified and interpreted in light of plate-wave theory [5,6]. Modal acoustic emission was shown to accurately determine when, where, and how much matrix cracking occurs in SiC/SiC composites tested in tension at room and elevated temperatures [7-9]. The same approach employed in these earlier studies on SiC/SiC composites for straight-sided tensile specimens was used to analyze curved C-coupon specimens tested in tension in this study.

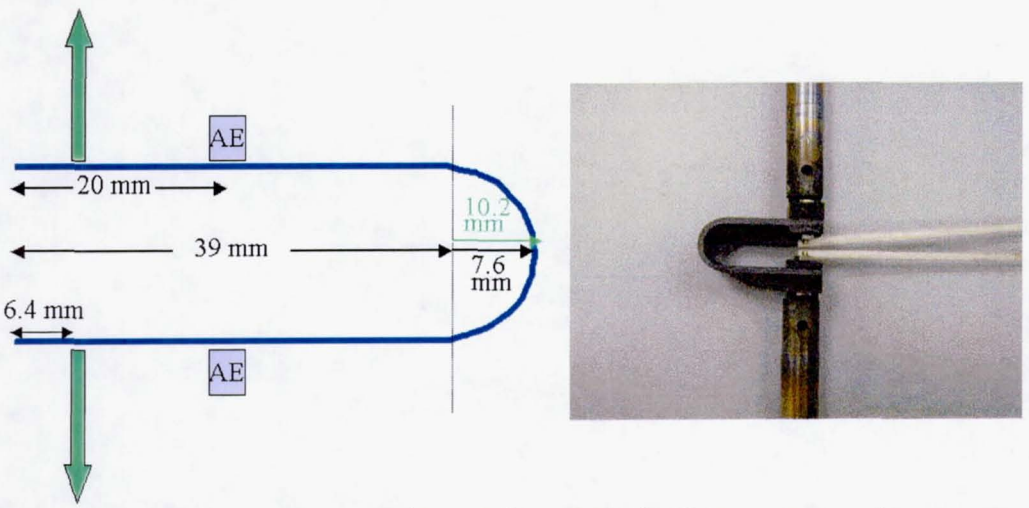

Figure 1: Schematic representation and photograph of a C-coupon test-specimen.

EXPERIMENTAL

A schematic representation and photograph of a C-coupon specimen is shown in Figure 1. The specimen geometry and testing was identical to that described in references 1 and 2. All tests were performed at Southern Research Institute (Birmingham, AL). Two 9 mm diameter wide-band AE transducers (B1025, Digital Wave Corporation, Englewood CO) were attached using spring loaded-clamps as shown in Figure 1. Vacuum grease was used as a couplant between the transducer and the specimen. For elevated temperature tests, 815°C, a smaller diameter (5 mm) wide-band transducer (B1080, Digital Wave Corporation) was attached at the end of a 75 mm steel waveguide (~ 5 mm diameter). AE was recorded during a test and later analyzed with a Fracture Wave Detector™ (Digital Wave Corporation) similar to the unit described in reference 7, except that the unit used in this study was portable and had a Pentium II processor. The tensile loading rate was 44.5 N/min. The test was stopped if a plateau or peak in the load-displacement curve occurred. Load was recorded by the AE system so that a given AE event could be associated with the applied load.

Five different SiC/SiC composite systems were studied composed of two different SiC matrices and three different fiber-types. Melt-infiltrated (MI) SiC C-coupon composite specimens were fabricated by Honeywell Advanced Composites (Newark, DE) with Dow-Corning Sylramic® and Ube Industries Tyranno ZMI fiber-types. These composite systems will be referred to as SYL-MI and ZMI-MI, respectively. Polymer-infiltration and pyrolysis (PIP) SiC C-coupon composite specimens were fabricated by COI Ceramics (San Diego, CA) with Sylramic, ZMI, and Nippon Carbon Hi-Nicalon™ fiber-types and their S200 and S300 matrices. These composite systems will be referred to as SYL-S300, ZMI-S200, and HN-S200, respectively. The individual specimens were sectioned from "logs" of material having an inner radius of ~ 7.6 mm and an outer radius of 10.2 mm. For some of the composite systems tested, specimens from more than one log were used. Polymer-derived materials were sectioned into individual coupons in the green state, and then re-infiltrated to final density.

RESULTS AND DISCUSSION

Sound Wave Propagation

Before C-coupon testing was performed, it was first established that acoustic wave propagation around the curved portion of the C-coupon specimen could be treated the same as a flat plate. Of most importance for this work was to determine if the speed of sound of the extensional wave (i.e. the first peak [7]) propagated around the curvature in the same mode as for a flat plate. The speed of sound of the extensional portion of the AE waveform was measured over a flat portion and over the curved portion of the specimen based on the simple relationship: $C_e = x/\Delta t$, where x is the distance along the length of the specimen between the two sensors and Δt is the difference in time of arrival for the first peak recorded on both sensors. The "length" of the curved portion of the specimen was based on the radius of curvature of the midline of the specimen, 8.9 mm. For each individual specimen tested, the speed of sound around the curved portion was always found to be within a few percent of the speed of sound in the flat region. However, the speed of sound differs from specimen to specimen due to differences in elastic modulus and density: $C_e \propto (E/\rho)^{1/2}$. For example, the speed of sound for SYL-MI was ~ 10,500 m/s whereas the speed of sound for SYL-S300 was ~ 8,000 m/s.

Next, several pencil lead breaks and 16 mil boron fiber (Textron Specialty Materials, Lowell, MA) breaks were performed at different predetermined locations on the outer surface of the curved section of the specimen with the AE sensor set-up shown in Figure 1. The location in the long direction of the specimen was then determined and found to be relatively accurate, i.e., the deviation between predicted location and actual location never being more than 3 mm. Therefore, the assumption that wave propagation can be approximated as a thin, flat plate is justified and can be used for source location determination.

C-Coupon Tensile Tests

The load-deflection curves for some of the room temperature C-coupon tests are shown in Figure 2. The initial portion of the loading curves for each composite system was relatively reproducible. There was some slight non-linearity early in the test but significant non-linearity in the load-displacement curve did not usually occur until higher loads. The ultimate loads were not always reproducible for the different composite systems.

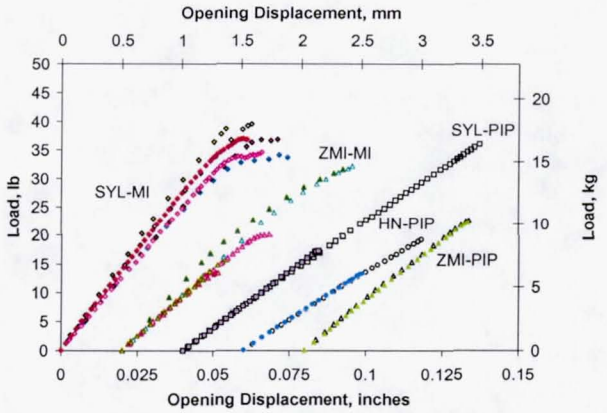

Figure 2: Load-displacement curves for C-coupon tests. The individual data is displaced on the x-axis for clarity.

Significant AE activity occurred during the tests usually over a relatively large load range. The data was sorted so that only the events that emanated from between the sensors were analyzed. Figure 3 shows the AE activity for a specimen with the least amount of AE activity, HN-S200

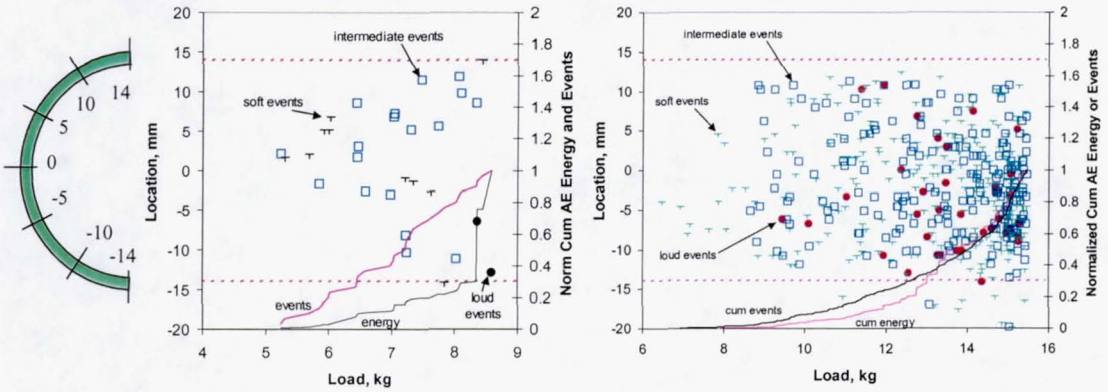

Figure 3: Location of AE events and normalized cumulative AE events and AE energy plotted versus increasing load for (a) HN-S200 C-coupon and (b) SYL-MI tests. Also shown is a schematic representation of the curved portion of the C-coupon and the longitudinal distance along the length of the specimen. The location equal to zero corresponds to the center of the curved portion of the C-coupon. Failure occurred at the end of AE activity.

(Figure 3a) and a specimen yielding the most AE activity, SYL-MI (Figure 3b), respectively. AE events are plotted versus the applied load. For all of the tests, the first event occurred within 5 mm of the center of the curved portion of the C-coupon. With increasing loads, AE events occur over a wider length of the curved portion of the specimen and appear to "fan" out from the first event location. Few if any events occur outside of the curved portion of the specimen, i.e. ± 14 mm. An increase in AE activity, especially the energy of events, occurs near the end of the tensile test prior to and at failure.

The first AE event always occurred in the region of predicted highest ILT stress, i.e., at mid thickness and within +/- 45° of the centerline [1]. Presumably, with increasing load, this interlaminar crack extends around the curved portion of the C-coupon and other interlaminar cracks form and extend at different depths and locations in the curved portion of the C-coupon. The rate of AE activity continues to increase with increasing load and the highest energy events tend to occur at higher loads. The higher energy events near the end of the test may correspond to the formation of transverse cracks and the linking up of interlaminar cracks that ultimately lead to the failure of the C-coupon. It should also be noted that for all of the specimens, except for SYL-S300, some AE events that occurred at higher loads had higher frequency contents compared to lower load AE events. This may also be indicative of transverse matrix cracks [9]. Both interlaminar matrix cracks at different locations through the thickness and transverse matrix cracks on the inner radius of the C-coupon were observed post-test for tested C-coupon specimens [10].

AE definitely provides the load range when matrix cracking occurs during a C-coupon test. Relating this load range to the determination of ILT strength will be considered in the next section. However, it would be useful to employ a graphical technique for assessing the load at which first cracking occurs if AE is not monitored. Two approaches were compared in this study: the 1st deviation from linearity and an offset-intercept method [11]. Figure 4 shows several C-coupon load-displacement curves for room temperature and elevated temperature tests as well as the load at which the first AE event was recorded in the curved section of the C-coupon. Also plotted is a linear regression fit of the load-displacement data. For some tests, there was slight non-

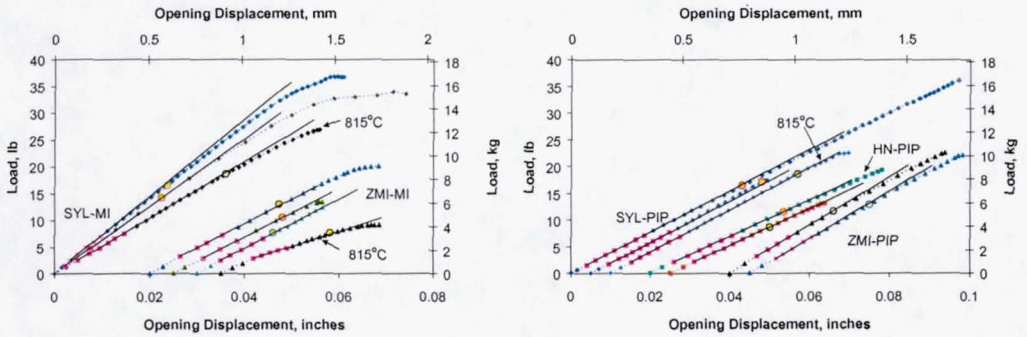

(a) (b)

Figure 4: Load-displacement curves C-coupon tests performed at room temperature and at 815°C (where labeled) for (a) MI composite specimens and for (b) PIP composite specimens. The circles represent the load for the first AE event in the curved portion of the C-coupon. The line represents the linear regression for the load-displacement data from 1 to 3.4 kg. When needed, the individual curves are displaced along the x-axis for clarity (except for SYL-MI data in a).

linearity up to ~ 1 kg due to alignment of the test fixture. Therefore, the data was regressed between 1 and 3.4 kg and the load at which the regressed line deviated from the load-displacement curve was noted. Then the slope of that regression fit was multiplied by 0.98 and 0.95 to determine the 98% and 95% offset slopes, respectively, and the load at which those lines intercepted the load-displacement curve were noted as the 98% offset intercept and the 95% offset intercept, respectively.

Figure 5 shows the loads for the 1st AE, deviation from linearity (1st non-linearity), and 95% and 98% offset intercept. In general, the 1st AE load correlates with the 98% offset intercept load or the 1st non-linearity load. The 1st AE load consistently correlated with the 98% offset intercept load for the MI specimens. The 1st AE load for the PIP specimens tended to vary between the 1st non-linearity load and the 98% offset intercept load. For two tests, the deviation from linearity was so minor that a 98% offset never intercepted the load-displacement curve.

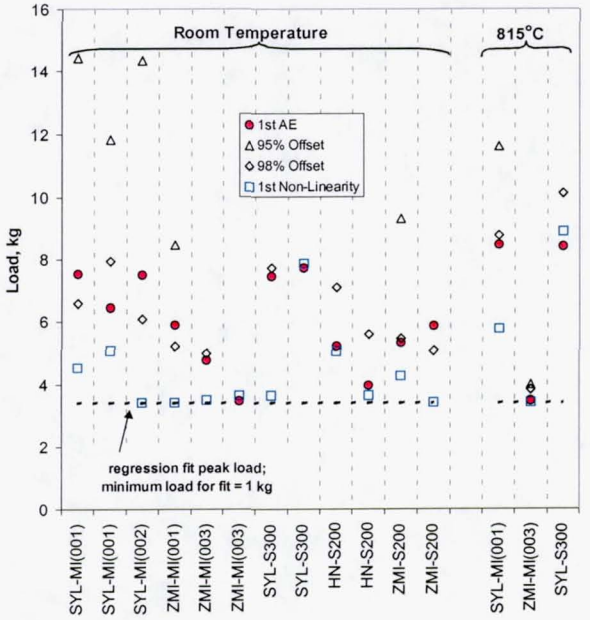

Figure 5: Load of 1st AE, non-linearity, and intercept of 98% and 95% offset slopes.

It should be noted that the use of waveguides for the elevated temperature tests did reduce the sensitivity for detection of AE. One room temperature test, ZMI-MI (003) #4, was performed with both waveguides and with the sensors directly attached to the specimen (Figure 1) before elevated temperature tests were performed in order to assess the loss in sensitivity. Only 11 events were recorded of events in the curved portion of the specimen with waveguides of the 53 events recorded by the directly attached sensors. The first event recorded with the waveguides was at a load of 4.8 kg compared to the 3.5 kg load for the first event recorded with the sensors directly in contact with the specimen. For the elevated temperature tests, the gain on the signal was amplified by 12dB, which appeared to increase the sensitivity of the waveguides. Unfortunately, no other specimens were available to compare the AE pick-up with directly attached sensors and it is therefore quite possible that the 1st AE load is an overestimate. However, it is significant that for the C-coupon tests performed at 815°C that the load for first AE with waveguides was in very good agreement with the 98% offset intercept load for MI specimens and the 1st non-linearity load for PIP specimens as was the case for room temperature tests with AE sensors in direct contact with the specimen.

Interlaminar Tensile Strength

The ILT stress was determined for the C-coupon specimens from the load for 1st cracking from AE, from the graphical techniques described above, and from the ultimate

failure load of the C-coupon test for each specimen using the equations derived in reference 1 and is plotted in Figure 6. Previous analytical work [1] demonstrated that, because the C-coupon specimen was statically determinate, the stress solution used to assess interlaminar fracture stress was insensitive to the differences in elastic properties of the composite systems considered in this study. Also shown in Figure 6 are data from tensile button tests for SYL reinforced composites [10], ZMI-S200 composites [10], and Nicalon™ fiber reinforced S200 matrix composites [12] for comparison. Although, Nicalon™ reinforced composites were not tested in this study, comparison of available Nicalon™-S200 button data and C-Coupon data for HN-S200 was compared in Figure 6.

The average first ILT cracking stress value determined for SYL composites was found to be ~ 7.1 MPa for both MI and S300 matrices. The average first ILT cracking stress for ZMI-MI was found to be ~ 4.6 MPa and for ZMI-S200 was found to be ~ 7.0 MPa. For HN-S200, the average first ILT cracking stress was determined to be ~ 5.4 MPa. The ILT strength measured from button tests was comparable to the ILT determined from the ultimate load of the C-coupon test for SYL reinforced composites. For the S200 matrix composites, ILT strength measured from a button test for the Nicalon™-S200 composite was more comparable to the average first ILT cracking stress of S200 matrix composites; whereas, ILT strength measured from a button test for the ZMI-S200 composite was nearly the same as ILT strength measured from the ultimate load of the C-coupon test.

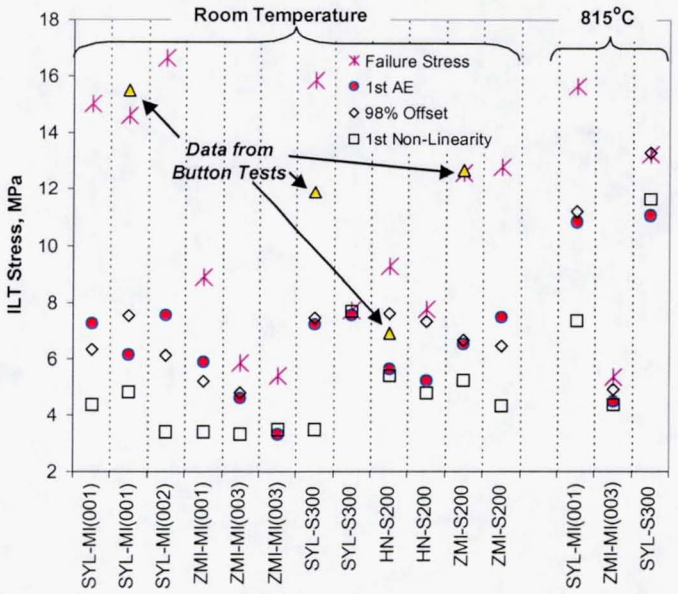

Figure 6: Interlaminar tensile strength determined from C-coupon tests. The data from tensile button tests was from references 10 and 12.

For the most part, this data indicates ILT strength from button tests best correlates with ILT strength from the ultimate load of a C-coupon test even though significant cracking had occurred in the C-coupon at lower stresses. It should be noted that the button test ILT values were performed on flat panels of different batches of material. Button tests from the "arms" of the same C-coupon specimens tested in this study are currently underway for a direct materials comparison between C-coupon test and button test ILT measurements. Interrupted C-coupon tests also need to be performed to confirm the extent of load-dependent damage occurring during the test. Finally, comparison of the two test methods will have to take into consideration (1) infiltration of the "C" shape may be different than that for flat panels (the ZMI coupons in particular showed large void formation in the radius region of the "C") and (2) possible hoop stress contributions to the ultimate load for the C-coupon.

SUMMARY AND CONCLUSIONS

Acoustic emission monitoring of C-coupon tests proved successful at determining the occurrence, location, and extent of matrix cracking during the C-coupon tests both at room and elevated temperatures. At elevated temperatures, wave-guides were used. The first AE event occurred in the highest interlaminar stress region of the specimen. With increasing loads it was determined that more events occurred in the same location and in locations progressing outward from the 1st AE event location. This corresponds well with the observation of multiple interlaminar and transverse cracks for a given failed C-coupon specimen. Graphical techniques were employed to estimate the load at 1st AE and it was found that this load usually occurred within the load range bounded by the load for initial non-linearity in the load-displacement curve and the load where the 98% offset of the linear regression fit intercepted the load-displacement curve. The ILT stress determined from the C-coupon test at first cracking (AE) load for SYL-MI was usually a significantly lower value than ILT strength measured from tensile button tests.

REFERENCES

1. A. Abdul-Aziz, A.M. Calomino, and F.I. Hurwitz, "Analysis of CMC C-Coupon Specimens for Structural Evaluation," *Ceram. Eng. Sci. Proc.*, **22** [3] 569-576 (2001)
2. F.I. Hurwitz, A.M. Calomino, A. Abdul-Aziz, and T.R. McCue, "C-Coupon Studies of CMCs: Fracture Behavior and Microstructural Characterization," *Ceram. Eng. Sci. Proc.*, **22** [3] 577-584 (2001)
3. R.Y. Kim and N.J. Pagano,"Crack Initiation in Unidirectional Brittle Matrix Composites," *Journal of the American Ceramic Society*, Vol. 74, No. 5, 1991, pp. 1082-1090.
4. Y-J Luo, S-C Chang, and I.M. Daniel, "Acoustic Emission Study of Failure Mechanisms in Ceramic Matrix Composites under Longitudinal Tensile Loading," *Journal of Composite Materials*, Vol. 29, 1995, pp. 1946-1961.
5. M.R. Gorman, "Plate Wave Acoustic Emission," *J. Acoust. Soc. Am.*, **90** [1] 358-64 (1991)
6. M.R. Gorman, "New Technology for Wave Based Acoustic Emission and Acousto-Ultrasonics," AMD-Vol. 188, Wave Propagation and Emerging Technologies, ASME, 1994:47-59.
7. G.N. Morscher, "Modal Acoustic Emission of Damage Accumulation in a Woven SiC/SiC Composite," *Composites Science and Technology*, Vol. 59, No. 5, 1999, pp. 687-697.
8. G.N. Morscher, "Modal Acoustic Emission of Damage Accumulation in Woven SiC/SiC at Elevated Temperatures," in Review of Progress in Quantitative Nondestructive Evaluation, Vol. 18A, D.O. Thompson and D.E. Chimenti, Eds., Kluwer Academic/Plenum Publishers, NY, 1999, pp. 419-426.
9. Morscher, G.N., "Use of Modal Acoustic Emission for Source Identification in Woven SiC/SiC Composites," Review of Progress in Quantitative Nondestructive Evaluation,, Vol. 19, , D.O. Thompson and D.E. Chimenti, Eds., American Institute of Physics, NY, 2000 pp. 383-390.
10. F.I. Hurwitz, A.M. Calomino, G.N. Morscher, and T.R. McCue, "C-Coupon Studies of SiC/SiC Composites Part II: Microstructural Characterization," to be published in this issue of *Ceram. Eng. Sci. Proc.*, **23** (2002)
11. M.G. Jenkins and L.P. Zawada, "Elastic Modulus and Proportional Limit Stress in Ceramic Matrix Composites: Comparison of Methods and Results," *Ceram. Eng. Sci. Proc.*, **22** [3] 503-511 (2001)
12. Unpublished data from COI Ceramics.